JACS
JOURNAL OF THE AMERICAN CHEMICAL SOCIETY
pubs.acs.org/JACS
Article

Cracking under Internal Pressure: Photodynamic Behavior of Vinyl Azide Crystals through N_2 Release

Dylan J. Shields, Durga Prasad Karothu, Karthik Sambath,[‖] Ranaweera A. A. Upul Ranaweera,[‖] Stefan Schramm, Alexander Duncan, Benjamin Duncan, Jeanette A. Krause, Anna D. Gudmundsdottir,* and Panče Naumov*

Cite This: *J. Am. Chem. Soc.* 2020, 142, 18565−18575

ABSTRACT: When exposed to UV light, single crystals of the vinyl azides 3-azido-1-phenylpropenone (**1a**), 3-azido-1-(4-methoxyphenyl)propenone (**1b**), and 3-azido-1-(4-chlorophenyl)propenone (**1c**) exhibit dramatic mechanical effects by cracking or bending with the release of N_2. Mechanistic studies using laser flash photolysis, supported by quantum mechanical calculations, show that each of the vinyl azides degrades through a vinylnitrene intermediate. However, despite having very similar crystal packing motifs, the three compounds exhibit distinct photomechanical responses in bulk crystals. While the crystals of **1a** delaminate and release gaseous N_2 indiscriminately under paraffin oil, the crystals of **1b** and **1c** visibly expand, bend, and fracture, mainly along specific crystallographic faces, before releasing N_2. The photochemical analysis suggests that the observed expansion is due to internal pressure exerted by the gaseous product in the crystal lattices of these materials. Lattice energy calculations, supported by nanoindentation experiments, show significant differences in the respective lattice energies. The calculations identify critical features in the crystal structures of **1b** and **1c** where elastic energy accumulates during gas release, which correspond to the direction of the observed cracks. This study highlights the hitherto untapped potential of photochemical gas release to elicit a photomechanical response and motility of photoreactive molecular crystals.

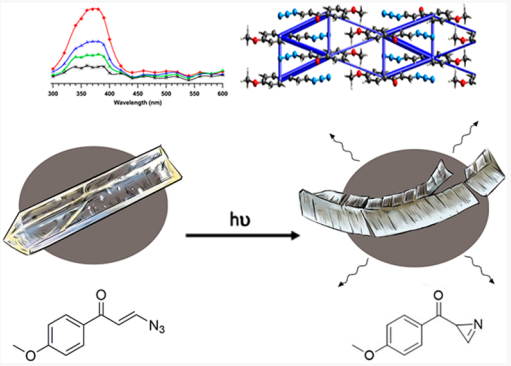

1. INTRODUCTION

The quest for new smart organic materials capable of transducing light and other stimuli into mechanical motion has intensified in recent years because of their potential in a number of applications, including electronics, biomedicine, and soft robotics. Specifically, these materials show promise for applications in smart sensors, electronics, and medical devices.[1−4] Historically, polymers and elastomers were among the first organic materials to be studied and applied as smart materials; however, owing to limitations associated with their disordered structures, there is now a demand for alternative materials endowed with long-range structural order that can transduce energy and respond faster while still being light in weight. Adaptive molecular *crystals* have recently been shown to be able to perform many of the same mechanical feats as their polymeric predecessors.[5−9] These previously underexplored materials can respond rapidly to external stimuli such as light, heat, or mechanical force by switching between different crystal packing arrangements (polymorphs) or by undergoing chemical reactions such as cyclization, *cis*−*trans* isomerization, or dimerization.[10] The underlying molecular reconfiguration generates a considerable strain in the crystal lattice, which is manifested as macroscopically visible motion such as bending, shattering, jumping, or flipping.[11]

An alternative, unexplored approach for eliciting motility in crystalline materials is to acquire momentum by releasing a gas, a mechanism that is analogous to the operation of a gasoline engine. A prominent recent example of crystal motion by gas release is the thermally induced coupling of a zwitterionic metal complex reported by Ovcharenko et al.[12−14]Although this phenomenon was attributed to the release of oxygen gas as a product of the reaction, the direct correlation of the reaction mechanism with the kinematic traits of the phenomenon was not conducted. Except for some early reports in some inorganic compounds,[15−19] other reports on mechanical movements caused by gas release are scarce, consisting of brief mentions or anecdotal reports in presentations. Thus, this study aimed to provide an in-depth understanding of the

Received: July 26, 2020
Published: September 29, 2020

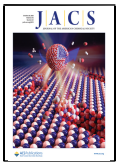

https://dx.doi.org/10.1021/jacs.0c07830
J. Am. Chem. Soc. 2020, 142, 18565−18575

photodynamic behavior of the crystals of three structurally related gas-releasing azido compounds (Chart 1) using a combined experimental and computational approach to study the underlying reaction mechanism. The crystals of 3-azido-1-phenylpropenone (**1a**), 3-azido-1-(4-methoxyphenyl)-propenone (**1b**), and 3-azido-1-(4-chlorophenyl)propenone (**1c**), whose molecular structures differ only by the *para*-substituent with respect to the ketone group, were found to have similar packing motifs but very different photomechanical responses. The driving forces responsible for crystal disintegration and motility were elucidated using video microscopy and by correlating the observed deformation, gas release, and motion to the structural and molecular modeling results. In addition to the kinematic study, the mechanism of denitrogenation was also investigated in solution and in the solid state through product studies and laser flash photolysis.

Chart 1. Molecular Structures of 3-Azido-1-phenylpropenone (1a), 3-Azido-1-(4-methoxyphenyl)propenone (1b), and 3-Azido-1-(4-chlorophenyl)propenone (1c)

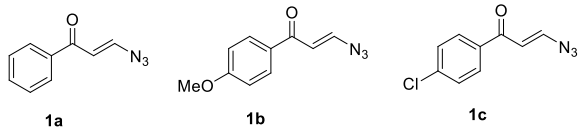

1a 1b 1c

2. RESULTS AND DISCUSSION

2.1. Product Analysis. The irradiation of the vinyl azides **1a−c** with UV light (Hg arc lamp) in argon-saturated chloroform-*d* resulted in the corresponding azirines **3**, isoxazoles **4**, and cyanides **5**, as depicted in Scheme 1. The reaction progress, followed by ^{1}H NMR spectroscopy, showed that the photoproduct ratio changed as a function of irradiation time, with continuous irradiation of the reaction mixture increasing the yield of cyanides **5** at the expense of azirines **3** and isoxazoles **4**. These results are in accord with the established photolysis behavior of **1a**.[20] In contrast, the irradiation of the crystals of vinyl azides **1a−c** pressed between glass slides selectively yielded azirines **3a−c**. As azirines **3a−c** are highly reactive, isolation using traditional column chromatography was not feasible. Instead, products **3**, **4**, and **5** were identified in the reaction mixture based on IR and NMR spectroscopic evidence. The recorded spectra of **4a−c** and **5a−c** were consistent with those available in the literature.[21−25] To support the characterization of azirines **3a−c**, we compared their ^{1}H NMR spectra to those reported for 2-benzoyl-2-methyl-2*H*-azirine and 2-methyl-2-phenyl-2*H*-azirine, in which the vinylic hydrogen atom on the azirine ring is observed at 9.75 and 9.80 ppm, respectively,[22] corresponding to that in azirine **3** at 9.67 ppm. Similarly, the α-hydrogen atom in azirine **3** is located at 3.5 ppm, which is similar to the chemical shift observed for the α-hydrogen atom of 2-benzoyl-3-methyl-2*H*-azirine at 3.50 ppm.[26]

Scheme 1. Photoproducts Obtained by Irradiation of Vinyl Azides 1 in Chloroform-*d* and as Crystals

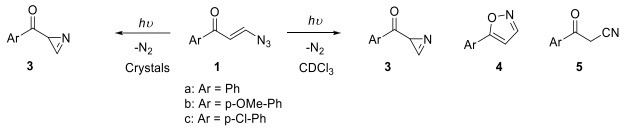

To further aid with characterization, thermolysis was performed in chloroform-*d* solutions of vinyl azides **1a−c** at 70 °C. The progress of the reaction was followed by ^{1}H NMR spectroscopy, which demonstrated that vinyl azides **1a−c** were cleanly transformed into azirines **3a−c** and cyanides **5a−c**. The ^{1}H NMR signals for the vinyl protons of vinyl azides **1a−c** at 6.5 and 7.5 ppm were depleted, and new signals for the protons on the azirine moiety appeared at 3.5 and 9.0 ppm. Thus, cyanides **5** are most likely formed both thermally and photochemically from azirines **3**. The product studies clearly demonstrated that the photoreactions in the crystals are more selective than their counterparts in solution. The formation of azirines in the solid state is presumably more favorable than the formation of isoxazoles as less molecular movement is required, which is preferable in a spatially constrained, rigid environment. This reasoning is consistent with the topochemical postulate, which states that solid-state reactions should proceed via the pathway of least molecular motion.[27] Based on the product formation, we theorize that upon exposure to light, vinyl azides **1a−c** form their corresponding singlet excited states (S_1) that intersystem-cross efficiently to triplet 1,2-biradicals ^{3}**2BR**, which then extrude a N_2 molecule to afford triplet vinylnitrene intermediates ^{3}**2N** (Scheme 2). Generally, triplet vinylnitrenes are short-lived intermediates that have significant 1,3-biradical character and intersystem-cross efficiently to form products.[28,29]

Scheme 2. Proposed Mechanism for the Formation of Photoproducts 3, 4, and 5 from Vinyl Azides 1

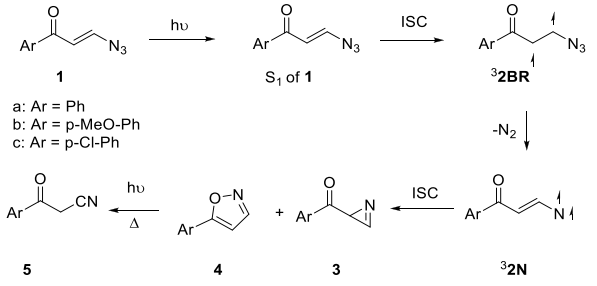

2.2. Laser Flash Photolysis. To verify that vinyl azides **1a−c** form products through vinylnitrene intermediates both in solution and in the solid state, we employed nanosecond laser flash photolysis studies. Laser flash photolysis of **1a−c** in argon-saturated acetonitrile gave transient spectra with absorption maxima between 340 and 360 nm (Figure 1A, Supporting Information Figures S1 and S2). The transient absorption was attributed to triplet vinylnitrene ^{3}**2N** based on a comparison with the TD-DFT-calculated absorption spectrum (Figure 1B) and the observation that the absorption is quenched in oxygen-saturated acetonitrile.

The decay of all transient absorptions in argon-saturated solutions were best fitted with a pseudo-first-order function, resulting in lifetimes of 10, 12, and 8 μs for vinylnitrenes ^{3}**2Na**, ^{3}**2Nb**, and ^{3}**2Nc**, respectively. The transient absorptions formed with rate constants of $\sim 2 \times 10^7$ s^{-1}, which correspond to the decay of the precursor 1,3-biradicals (^{3}**2BR**). The laser flash photolysis studies demonstrate that solution photolysis of vinyl azides **1a−c** results in the formation of triplet vinylnitrenes and that the *p*-substituent does not significantly

https://dx.doi.org/10.1021/jacs.0c07830
J. Am. Chem. Soc. 2020, 142, 18565−18575

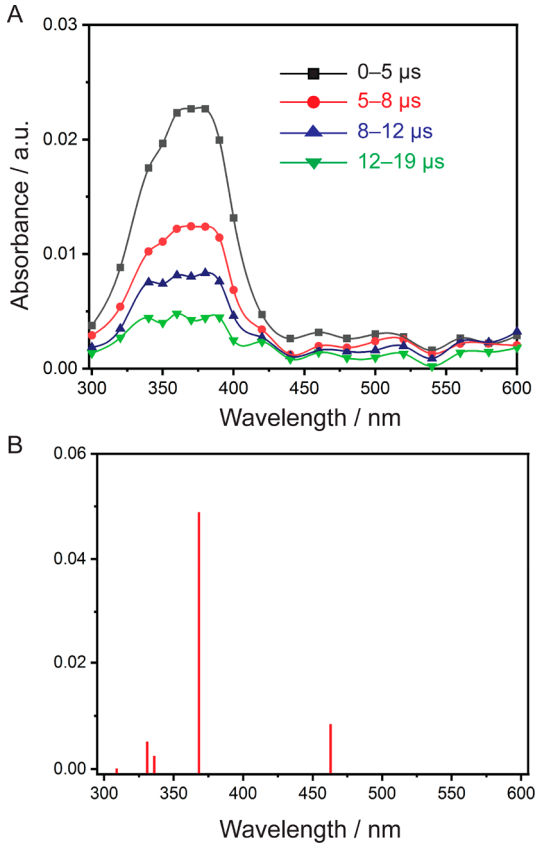

Figure 1. (A) Transient spectra obtained by laser flash photolysis of **1b** in argon-saturated acetonitrile. (B) TD-DFT-calculated line spectrum of vinylnitrene ^{3}**2Nb** using C-PCM solvation and acetonitrile.

affect the reactivity while only slightly affecting the absorption profile.

The laser flash photolysis of vinyl azides **1** was performed in nanocrystalline suspensions in accordance with literature procedures.[30] The transient absorption spectra obtained by laser flash photolysis of crystalline **1a–c** (Figure 2) are similar to those obtained in solution with absorbance maxima between 350 and 380 nm, which are attributed to triplet vinylnitrenes ^{3}**2Na–c**. However, the nanocrystalline suspension spectra are not fully quenched when the suspension is saturated with oxygen or air, presumably because the quenching mechanism in crystals is less efficient than in solution. Furthermore, an analysis of the kinetics in argon-saturated suspensions revealed that vinylnitrenes ^{3}**2Na**, ^{3}**2Nb**, and ^{3}**2Nc** are longer lived than in solution, with lifetimes of 14, 12, and 14 μs, respectively. In comparison, in air- and oxygen-saturated nanocrystalline suspensions, the lifetimes of the triplet vinylnitrenes are reduced but not completely quenched. Importantly, the rate of formation of the vinylnitrenes from nanocrystalline suspensions of vinyl azides **1** became faster than the time resolution of the laser. Altogether, the laser flash photolysis studies of vinyl azides **1a–c** in nanocrystals demonstrate that, in crystals, triplet vinylnitrenes are formed faster, are longer lived, and are less easily quenched by oxygen. However, vinylnitrenes ^{3}**2Na–c** have remarkably similar lifetimes in the solid state.

2.3. Quantum Chemical Calculations. To further explore the photoreactivity of vinyl azides **1**, TD-DFT calculations of their reactions were carried out using the B3LYP method in conjunction with the 6-31+G(d) basis

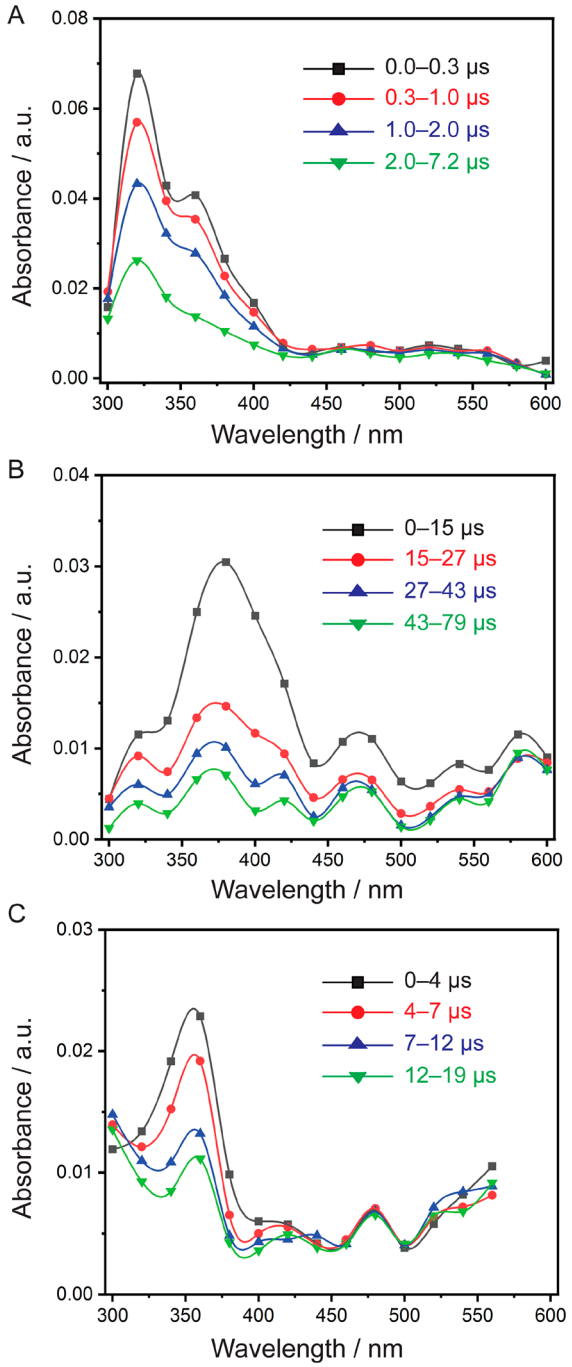

Figure 2. Transient spectra obtained by laser flash photolysis of (A) **1a**, (B) **1b**, and (C) **1c** in argon-saturated nanocrystalline suspensions.

set.[31,32] The optimized minimal energy conformer of vinyl azide **1a** showed that the molecule is fully conjugated and flat (Figure 3). The S_1 state of **1a** was calculated by TD-DFT to be 76 kcal mol^{-1} higher in energy than its ground state (S_0) (Figure 4, left). The optimization of the triplet configuration of vinyl azide **1a** revealed that it is best described as a 1,2-biradical, ^{3}**2BRa** (Figure 3). The minimal energy conformer of **2BRa** is 55 kcal mol^{-1} above its S_0 state (Figure 4A), and spin density calculations located the unpaired electrons on the C_α and C_β atoms, which were rotated ~90° away from each other to minimize the overlap between the radical centers (Figure 4B). The optimization of the structure of vinylnitrene ^{3}**2Na**

https://dx.doi.org/10.1021/jacs.0c07830
J. Am. Chem. Soc. 2020, 142, 18565–18575

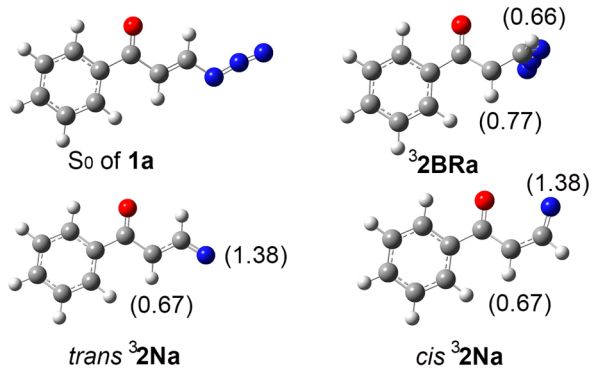

Figure 3. Optimized structures of **1a**, ^{3}**2BRa**, and two isomers of ^{3}**2Na**. The numbers in the parentheses are the calculated spin densities.

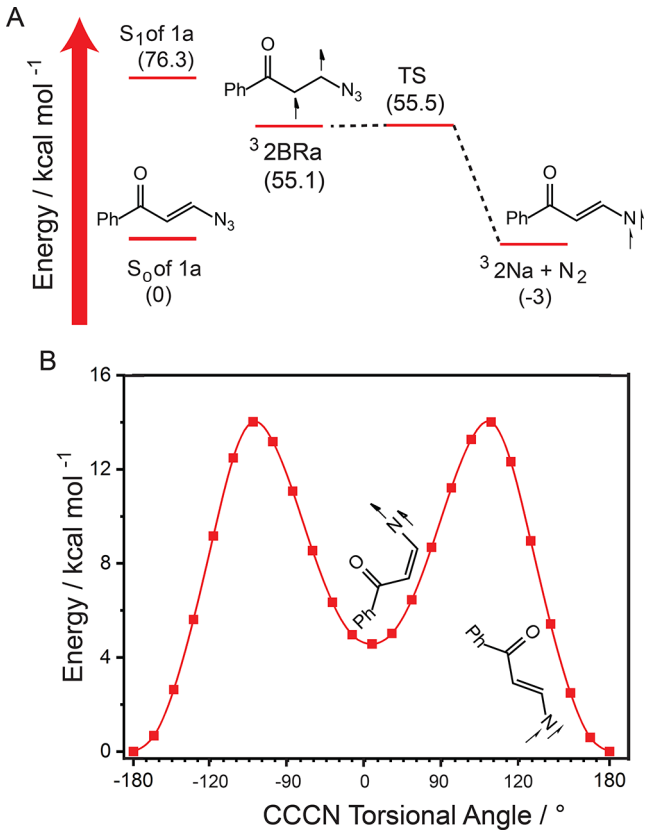

Figure 4. (A) Calculated stationary points on the triplet surface of **1a**. The energies are in kcal mol^{-1}. (B) Calculated rotational barrier for ^{3}**2Na**.

showed that this species exists as two conformers (*trans* and *cis*, Figure 3) corresponding to two energy minima, with the *trans* isomer being 5 kcal mol^{-1} more stable than the *cis* isomer (Figure 4A). Furthermore, spin density calculations showed that vinylnitrene ^{3}**2Na** has a significant 1,3-biradical character, and the rotational barrier around the vinylic bond is low (~14 kcal mol^{-1}) (Figure 4B). The calculated transition state barrier for the transformation of ^{3}**2BRa** to vinylnitrene ^{3}**2Na** was found to be very small (0.4 kcal mol^{-1}). Therefore, the calculations support the hypothesis that vinylnitrene ^{3}**2Na** is easily formed from the excited state of vinyl azide **1a**. Structural flexibility can explain the formation of both azirine **3a** and isoxazole **4a** in solution. The stationary points on the triplet surfaces of vinyl azides **1b** and **1c**, calculated using DFT, resulted in a similar diagram as that for vinyl azide **1a** (Supporting Information Figures S3 and S4). Furthermore, the calculated rotational barriers for vinylnitrenes ^{3}**2Nb** and ^{3}**2Nc** were comparable to that for vinylnitrene ^{3}**2Na** (Supporting Information Figures S5 and S6).

2.4. Photomechanical and Disintegrative Effects. When the crystals of vinyl azide **1a** were exposed to a 400 nm LED and monitored using an optical microscope equipped with a camera, they were observed to fragment, shatter, and splinter violently as a result of the photochemical reaction (Figure 5A, Supporting Information Video 1). As the reaction

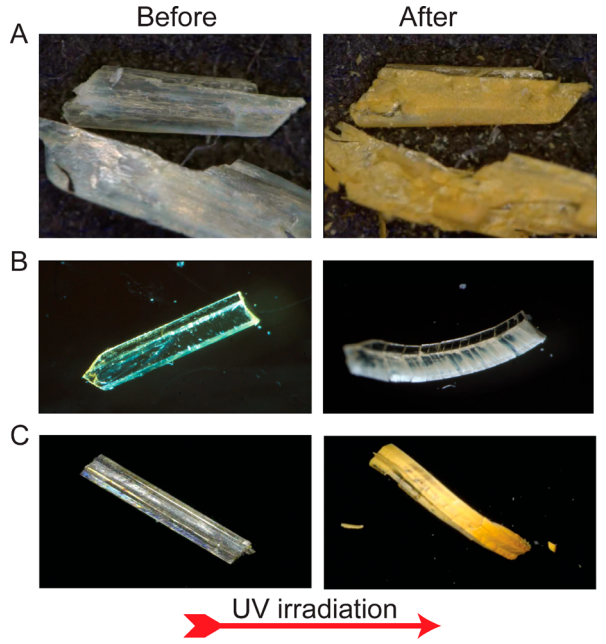

Figure 5. Optical microcopy images showing the photomechanical effects, cracking, and disintegration during the photochemical reactions of the crystals of **1a**–**c**. (A) Splintering of a crystal of **1a** upon irradiation. The approximate size of the crystal is ~1.6 × 0.5 × 0.1 mm^3. (B) Bending of the crystal of **1b** and development of parallel striations on the crystal surface due to cracking. The approximate size of the crystal is ~1.5 × 0.3 × 0.1 mm^3. (C) Bending and cracking of a crystal of **1c**. The approximate size of the crystal is ~2 × 0.5 × 0.2 mm^3. For recording of the effects, see Supporting Information Videos 1–7.

progressed, the color of the translucent crystals and the debris changed from colorless to opaque amber. Due to violent fracturing of the crystals, the resulting debris had irregular and defective surfaces, and was not amenable to nanoindentation to determine their mechanical properties. To observe the evolution of gas, the crystals of azide **1a** were covered with mineral oil and irradiated. The released N_2 appeared as bubbles emanating from the crystal (Supporting Information Video 2). The bubbles formed and evolved from the crystals without a clear preference with respect to their edges or visible defect sites.

In stark contrast, the crystals of **1b** were observed to visibly bend, expand, and then crack (Figure 5B, Supporting Information Video 3). Moreover, if they were not restrained, some of these crystals jumped off the surface (Supporting Information Video 4); however, no splintering or violent fragmentation was observed. At this point, it is not clear

https://dx.doi.org/10.1021/jacs.0c07830
J. Am. Chem. Soc. 2020, 142, 18565−18575

whether the expulsion of gas or the disintegration of the lattice is responsible for the acquired motility of the crystals and the ensuing debris. Since the crystal explosion occurs almost concomitantly with the gas release, these effects cannot be resolved by simple kinematic analysis. Another distinct difference was that the cracks in the crystals of **1b** always developed perpendicular to the (010) face. When the irradiation of **1b** was performed in mineral oil, the crystals retained the gaseous N_2 before eventually releasing it at one of the cracks on the (010) face. Occasionally, the formation of a gas bubble could be observed in the crystal prior to cracking (Figure 6, Supporting Information Video 5). The crystals of **1c**

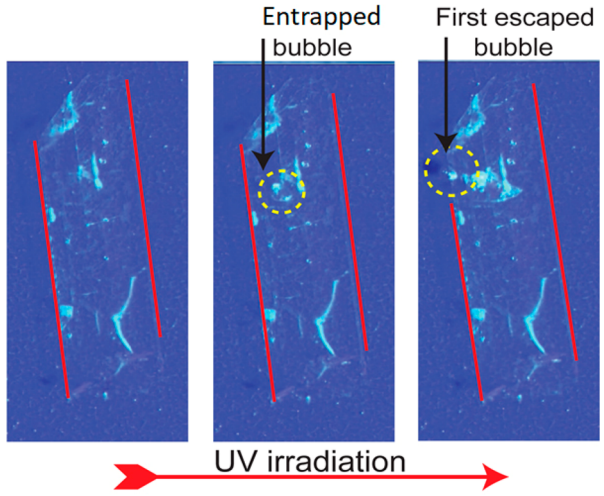

Figure 6. Formation of a bubble inside a crystal of azide **1b** and its subsequent release. Owing to the transparent nature of the crystal, red lines have been added to highlight a pair of parallel crystal edges. See Supporting Information Video 5.

behaved similarly to those of **1b**, in that exposure to light resulted in bending, expansion, and cracking (Figure 5C, Supporting Information Video 6) as well as some jumping (Supporting Information Video 7). The cracks in the crystals of **1c** also formed perpendicular to the long axis, allowing for the release of N_2 gas. The behavior of the crystals of **1c** in oil resembles that of the crystals of **1b**, with no N_2 released from the crystal until cracks develop in the interior that appear as striations on the surface (Supporting Information Video 8).

2.5. Crystal Structures and Mechanical Properties. The crystal structures of vinyl azides **1a–c** were determined and inspected for clues that may help elucidate the origin of the photomechanical effects. The crystals of vinyl azides **1a** and **1b** were both found to belong to the monoclinic $P2_1/n$ space group, whereas the crystals of **1c** were in the triclinic $P\bar{1}$ space group. The intramolecular atomic distances are very similar in all three compounds, generally falling within the range ±0.1 Å for C=C, C–C(O), and C–N_3 bonds (Crystallographic Supporting Information). The main structural difference in molecular geometries was the torsion angle between the *ortho* carbon of the phenyl ring and the carbonyl oxygen; **1a** and **1b** have planar torsion angles of ≤1°, whereas that in **1c** is 11° (Supporting Information Figures S7–S10). In the crystals, the molecules of **1a–c** pack in sheet-like motifs (Figure 7). The centroid-to-centroid distances between the phenyl rings are all in the range 3.80–3.87 Å, suggesting weak π–π interactions. The shortest distance between the vinyl moieties (C_α-to-C_α, C_β-to-C_β, N_1-to-N_1, N_2-to-N_2, and N_3-to-N_3) of adjacent molecules are also similar for **1a** and **1b**. As the crystal packing of the three compounds is very similar, it cannot account for the differences in their photodynamic behavior.

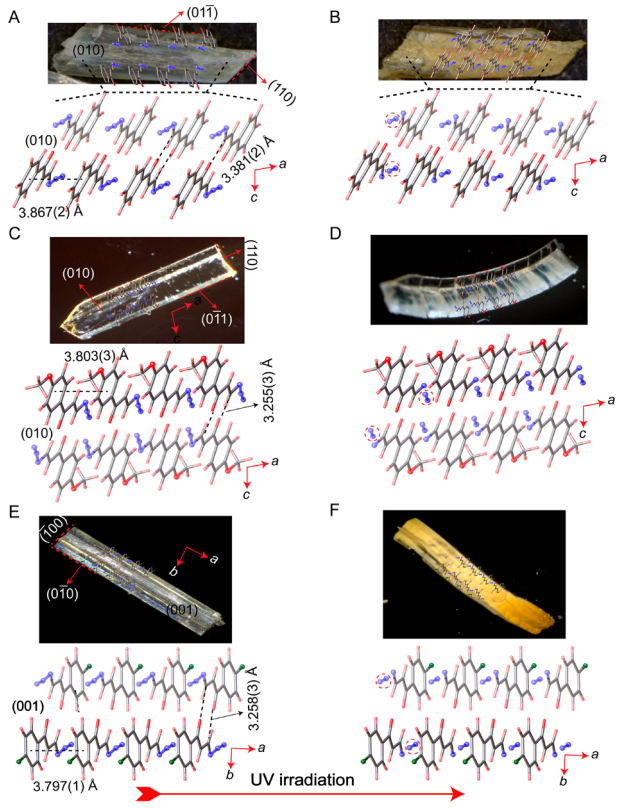

Figure 7. Molecular packing in the crystals of compounds **1a–c** before and during reaction, and correlation with the mechanical effects. (A,C,E) Superimposition of an optical images of single crystals of **1a** (A), **1b** (C), and **1c** (E) and the respective crystal structures before irradiation. (B,D,F) Optical images of the crystals of **1a** (B), **1b** (D), and **1c** (F) after irradiation, and model of the respective crystal structures at the initial stage of nitrogen release, before significant structure perturbation occurs. The channels are shown between the molecular columns where the nitrogen molecules are likely to accumulate before pressure builds up and induces peeling, bending and cracking of the crystals.

The faces of typical crystal habits were indexed and related to the respective crystal structures to identify any preferred directions in the crystals for reactivity, bending, and gas release. As expected from the crystal symmetries, the crystal faces of **1c** are different from those of **1a** and **1b** (Figure 7). A comparison of the packing diagrams and crystal faces indicated that **1b** and **1c** first show cracking on the (010) and (001) faces, respectively, whereas **1a** does not show a preferential face for chipping or cracking. The directionality of cracking in **1b** and **1c** can be rationalized by considering the intermolecular interactions. If the interactions are sufficiently strong to overcome the elastic energy, the gas remains inside the crystal during the course of the photochemical reaction. It accumulates until a threshold in the elastic energy is reached and a crack is generated. The gas is expected to accumulate preferentially at locations in the crystal where the interactions are weakest or in any voids or channels in the structure. As more gas is generated, it eventually reaches the surface of the crystal, which is the (010) and (001) face for **1b** and **1c**, respectively. With this qualitative scenario in mind, the

https://dx.doi.org/10.1021/jacs.0c07830
J. Am. Chem. Soc. 2020, 142, 18565–18575

structure diagrams in Figure 7 indicate that all three crystal structures contain channels owing to their sheet-like packing motifs. The channels provide preferred sites for accumulation of gas. Being effective concentrators of the accumulated elastic energy, the first cracks are expected to appear at surface imperfections or other crystal defects that alleviate the stability of the lattice. This reasoning implies that the origin of the photomechanical motions lies within the difference in lattice energetics between the three crystals; **1a** probably lacks sufficient energy to prevent cracking, whereas **1b** and **1c** likely possess more energy owing to their resistance to cracking. In an attempt to determine the structure of the products while they were generated inside the crystal interior, we resorted to X-ray photodiffraction (photocrystallography) by using different conditions. However, these efforts remained fruitless due to the proclivity of the crystal to crack and partially or completely disintegrate before significant amounts of the product could be generated for data collection and structure determination.

Because the deformation is related to mechanical compliance of the crystal, nanoindentation experiments were performed to determine if the crystal stiffness and hardness could explain the differences in the mechanical motions with gas release. Vinyl azides **1b** and **1c** were found to have elastic (Young's) moduli of 9.8 ± 0.5 GPa and 8.1 ± 0.7 GPa, respectively (Figure S11). Attempts to obtain the elastic modulus of **1a** were unsuccessful owing to the brittle nature of its crystals. This result indicates that **1b** and **1c** are likely to have higher stiffnesses, which was subsequently confirmed using lattice energy calculations.

2.6. Lattice Energy Calculations. As lattice energies and anisotropy of intermolecular interactions appear to be the key to explaining the different photomechanical effects, the so-called energy frameworks[33] were calculated to provide a more quantitative description and to visualize the anisotropy of the intermolecular interactions in the crystals. The results, in Figure 8, showed that **1a** features significantly weaker crystal interactions than **1b** and **1c**. In **1a**, the strong interactions ranged between 15.2 and 33.9 kJ mol^{-1} with weaker interactions of 6 kJ mol^{-1}. In comparison, **1b** had strong interactions ranging from 13.2 to 40.6 kJ mol^{-1} and weak interactions of 11.7−12.9 kJ mol^{-1}. Similar to **1b**, **1c** had strong interactions of 18.4−41.5 kJ mol^{-1} and weak interactions of 7.8−10.1 kJ mol^{-1}. These differences in the energy framework are responsible for the differences in the strength toward cracking between the weak, flaky crystals of **1a** and the strong, mechanical crystals of **1b** and **1c**. The observation that **1b** and **1c** crack along a specific crystal face during irradiation implies that N_2 gas is released within the crystals at locations where the intermolecular interactions are weakest. Support for this hypothesis is drawn from the correlation among the lattice energy calculations, crystal face indexing, and nanoindentation measurements.

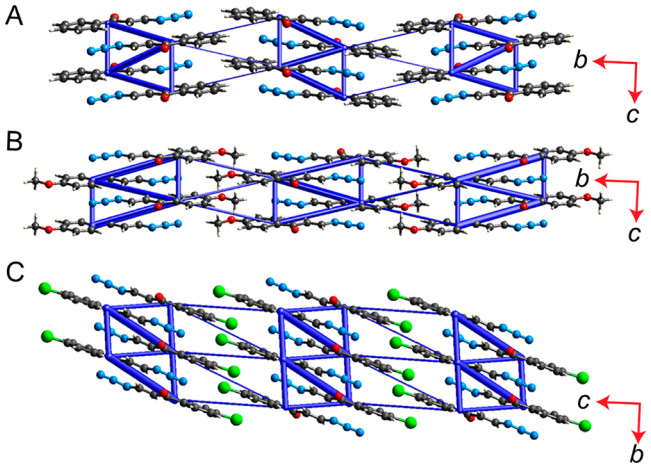

Figure 8. Energy frameworks of vinyl azides **1a**−**c** (tube size = 80, energy cutoff = 5 kJ mol^{-1}). (A) **1a** has weak interactions of 6 kJ mol^{-1} and strong interactions of 15.2−33.9 kJ mol^{-1}. (B) **1b** has weak interactions of 11.7−12.9 kJ mol^{-1} and strong interactions of 13.2−40.6 kJ mol^{-1}. (C) **1c** has weak interactions of 7.8−10.1 kJ mol^{-1} and strong interactions of 18.4−41.5 kJ mol^{-1}.

Vinyl azide **1a** does not exhibit a preferential cracking direction. Instead, crystal surface delamination or random shattering occurs upon irradiation. Correspondingly, the lattice energy calculations showed that this compound has the weakest interactions. These very weak interactions cannot keep the crystal together effectively, resulting in random delamination and shattering. This observation is supported by the nanoindentation experiments, which confirmed that the crystals of **1a** were too brittle to provide a proper basis for crystal indentation. Lastly, the void spaces in this crystal are located near the area with the weakest lattice energy interactions. The void space location is significant because as the pressure of N_2 increases in these void spaces, the likelihood of overcoming the weak forces in this area increases, allowing cracks to appear.

In contrast, when the crystals of **1b** are irradiated, they consistently break along their (010) face. When this observation is compared to the lattice interaction calculations, as shown in Figure 8, the repeated cracks can reasonably be attributed to the breakdown of the weak interactions between the methoxy groups, which are the weakest interactions identified by the lattice energy calculations. Because these weak interactions are stronger than those in **1a**, the crystals of **1b** maintain their form and shape more effectively upon the release of nitrogen gas. This behavior is supported by the nanoindentation experiments, which showed that the crystals of azide **1b** had the highest Young's modulus. Again, the location of the void space corresponds well with the location of the weak interactions in the crystal, suggesting that the growing N_2 volume will eventually overcome the weak interactions.

Similar results were obtained when this rationale was applied to **1c**. However, unlike those of **1b**, upon irradiation the crystals of **1c** crack perpendicular to the (001) face. When the lattice energy calculation is rotated perpendicular to the *c* axis to imitate this cracking action, the spaces in the cracks again align with the weak interactions between the chlorine substituents between the layers. Furthermore, the chlorine interactions are weaker than the methoxy interactions, which is supported by the nanoindentation data, which showed that **1c** had a lower Young's modulus than **1b** but presumably a higher Young's modulus than **1a**. These weaker interactions are evident in the video showing the decomposition of **1c** (Supporting Information Video 7), in which the crystal shape is mostly maintained, similar to the crystals of **1b**, but some crystals fragment and shatter, like the crystals of **1a**. This behavior is in line with the weak lattice points identified by the lattice energy calculations being intermediate between those in **1a** and **1b**.

https://dx.doi.org/10.1021/jacs.0c07830
J. Am. Chem. Soc. 2020, 142, 18565−18575

3. CONCLUSIONS

The reaction mechanism and photomechanical effects of vinyl azides **1a−c** were thoroughly investigated. To the best of our knowledge, this is the first in-depth study of crystal disintegration and movements induced by gas release where the photomechanical effects are directly correlated with the structure in a set of structurally similar compounds. While the mechanistic details of the photochemical reactions in these crystals are well established from the transient spectra and the crystal structures of the unreacted crystals provide a solid basis to hypothesize the origin of the mechanical effects, the relation with the mechanical effect should be considered with some precaution. Namely, the three key processes—the photochemical reaction that results in formation and accumulation of gas, the formation of cracks, and finally the crystal explosion—occur on very different time scales that cover several orders of magnitude. The kinetics of the mechanical response is unlikely to follow the kinetics of the photochemical reaction because the formation of cracks requires accumulation of gaseous product and buildup of pressure up to a threshold value. Since the quantum yield of the reaction is low, this process requires a significant amount of time and occurs on a much longer time scale than the photochemical reaction generating the gas. As a consequence, the mechanical response is much slower and has it own kinetics, which is additionally affected by the ensuing release of gas. This work highlights the relevance of different intracrystalline forces that determine the mechanical effects as a result of release of gas molecules. These and other gas-releasing crystals could be of significant use to researchers looking to create single-crystalline machines, where the momentum generated by the gas propels a crystal as a macroscopic entity. These "crystalline machines" would represent the macroscopic versions of molecular and nanoscale robots that operate via gas-generating chemical reactions.

4. EXPERIMENTAL SECTION

4.1. Calculations. The geometries of all structures were optimized using the B3LYP level theory with a 6-31G+(d) basis set with Gaussian16 software.[31,32,34] Absorption spectra of reactants, intermediates, and products were obtained using TD-DFT calculations using the C-PCM solvation method and acetonitrile.[35−37] Transition states were confirmed by analysis of one imaginary vibrational frequency as determined by the second derivative of the energy with respect to the optimized internal coordinates. The geometry of the transition state was also determined to be at a maximum of energy between the reactant and product by Internal Reaction Coordinate (IRC) calculations.[38,39] All calculations were performed at the Ohio Supercomputer Center.

4.2. Laser Flash Photolysis. Laser flash photolysis in solution and the solid state were performed with a laser flash photolysis apparatus connected to an excimer laser (308 nm, 17 ns).[40] The system at the University of Cincinnati is a commercial XE-LMP Luzchem system using a Lambda Physik LPX 100 Excimer laser at 308 nm with a 17 ns resolution. For solution laser flash photolysis, stock solutions of derivatives **1a**, **1b**, and **1c** in acetonitrile were prepared with an absorption between 0.3 and 0.8 at 308 nm. Solid-state nanocrystalline suspensions are prepared following the procedure by Simoncelli et al.[30] A saturated acetone solution of **1a**, **1b**, or **1c** was added to a water solution in a volumetric flask placed in a ultrasound bath, until the absorption at 308 nm was between 0.3 and 0.8. The samples were placed in a quartz cuvette with a 10 mm × 10 mm cross section, and for measurements obtained in argon- or oxygen-saturated acetonitrile and suspentions, the cuvettes were capped with a rubber septum and the appropiate gas was bubbled through them for 5 min. Transient absorption spectra were produced by plotting absorbance values that had been averaged from the kinetic traces at 20 nm intervals from 300 to 600 nm over the specified time intervals. Kinetic information was determined by plotting averaged kinetic profiles from specified wavelength and fitting the kinetic profiles with Igor Pro data software produced by WaveMetrics.

4.3. Preparation of Starting Materials. *4.3.1. Synthesis of 1-Phenyl-prop-2-yn-1-ol.* We followed the procedure reported in the literature by Chassaing et al. and Pigge et al. with some modifications.[41,42] To a solution of benzaldehyde (2.05 g 18.9 mmol) in 25 mL of anhydrous THF at 0 °C was added a solution of ethynylmagnesium bromide (48 mL 24 mmol, 1.2 equiv) in 15 mL of anhydrous THF. The mixture was stirred for 20 h at 0 °C, and the reaction was quenched by adding NH_4Cl (30 g of NH_4Cl dissolved in 100 mL of H_2O); the resulting mixture was stirred for 1 h. The solvent was removed under vacuum, and the residue was extracted with diethyl ether (100 mL). The diethyl ether layer was washed twice with water and once with brine (saturated NaCl) and dried over anhydrous $MgSO_4$. The diethyl ether was evaporated under vacuum to yield crude 1-phenyl-prop-2-yn-1-ol (2.0 g, 15.2 mmol, 78% yield). ^{1}H NMR, ^{13}C NMR, and IR spectra of the product were consistent with those reported.[41] ^{1}H NMR (400 MHz, $CDCl_3$): δ 2.38 (broad, 1H), 2.67 (d, J = 2.4 Hz, 1H), 5.46 (d, J = 2.4 Hz, 1H), 7.32−7.41 (m, 3H), 7.55 (d, J = 7.2 Hz, 2H) ppm; ^{13}C NMR (100 MHz, $CDCl_3$): δ 64.4, 74.9, 83.5, 126.6, 128.6, 128.7, 140.0 ppm; IR ($CDCl_3$): 3291, 3064, 3033, 2118, 1493, 1455, 1022, 1002, 947, 916, 698, 650 cm^{-1}.

4.3.2. Synthesis of 1-(4-Methoxy-phenyl)-prop-2-yn-1-ol. The same procedure was followed for the synthesis of 1-phenyl-prop-2-yn-1-ol.[41,42] A reaction of *p*-methoxybenzaldehyde (2.65 g, 19.5 mmol) with ethynylmagnesium bromide (48 mL, 24 mmol, 1.2 equiv) resulted in 4-methoxy-phenyl)-prop-2-yn-1-ol (**2a**) (2.73 g, 16.8 mmol) in 86% yield. The ^{1}H NMR, ^{13}C NMR, and IR spectra of the product compare well with those in the literature.[43,44] ^{1}H NMR (400 MHz, $CDCl_3$): δ 2.49 (broad, 1H), 2.66 (d, J = 2 Hz, 1H), 3.80 (s, 3H), 5.40 (d, J = 2 Hz, 1H), 6.90 (d, J = 8.4 Hz, 2H), 7.46 (d, J = 8.4 Hz, 2H) ppm; ^{13}C NMR (100 MHz, $CDCl_3$): δ 55.4, 64.0, 74.6, 83.8, 114.0, 128.1, 132.4, 159.8 ppm; IR ($CDCl_3$): 3397, 3288, 3005, 2959, 2838, 2116, 1611, 1588, 1512, 1250, 1175, 1112, 1031, 913, 833 cm^{-1}.

4.3.3. Synthesis of 1-(4-Chloro-phenyl)-prop-2-yn-1-ol. 1-Phenyl-prop-2-yn-1-ol was prepared in a similar manner as described above.[41,42] A reaction of *p*-chlorobenzaldehyde (1.50 g, 10.7 mmol) with ethynylmagnesium bromide (48 mL, 24 mmol, 1.2 equiv) resulted in 4 chloro-phenyl)-prop-2-yn-1-ol (1.7 g, 10.3 mml) in 96% yield. The NMR spectra of this compound were similar to previous literature values.[45] ^{1}H NMR (400 MHz, $CDCl_3$): δ 2.45 (broad, 1H), 2.66 (d, J = 2.0 Hz, 1H), 5. 40 (d, J = 2.0 Hz, 1H), 7.32 (d, J = 7.6 Hz, 2H), 7.46 (d, J = 7.6 Hz, 2H) ppm. ^{13}C NMR (100 MHz, $CDCl_3$): 61.8, 75.0, 82.3, 128.3, 128.8, 132.8, 137.3 ppm. IR ($CDCl_3$): 3297, 1594, 1575, 1273, 1191, 1032, 955, 818, 757, 645 cm^{-1}. GC/MS (EI): m/z 168, 167, 166, 149, 139, 131 (100), 113, 103, 77, 65.

4.3.4. Synthesis of 1-Phenyl-propynone. 1-Phenylpropyone was prepared using a similar method to that by Pigge et al. with some modification.[42] Jones reagent was prepared by mixing CrO_3 (4 g, 0.04 mol) with 4 mL of conc. H_2SO_4 to yield a slurry, to which water (3 × 4 mL) was added.[26] The Jones reagent was added dropwise to 1-phenyl-prop-2-yn-1-ol (2.0 g, 15.2 mmol) dissolved in acetone (25 mL) at 0 °C, over a period of 10 min until the color of the solution changed to green and then to orange. The mixture was stirred for 30 min, and the solvent removed under vacuum. The resulting residue was extracted with diethyl ether (100 mL). The ether layer was washed twice with water (100 mL), once with saturated $NaHCO_3$ (100 mL), and once with saturated brine solution (100 mL) and dried over anhydrous $MgSO_4$. The diethyl ether was evaporated under vacuum to yield crude 1-phenyl-propynone (1.38 g, 10.6 mmol) in 70% yield. ^{1}H NMR, ^{13}C NMR, and IR spectra of this compound correspond with the literature.[46,47] ^{1}H NMR (400 MHz, $CDCl_3$): δ 3.45 (s, 1H), 7.51 (t, J = 7.8 Hz, 2H), 7.66 (t, J = 7.4 Hz, 1H), 8.18 (d, J = 8.4 Hz, 2H) ppm.; ^{13}C NMR (100 MHz, $CDCl_3$): δ 80.3, 80.8,

https://dx.doi.org/10.1021/jacs.0c07830
J. Am. Chem. Soc. 2020, 142, 18565−18575

128.7, 129.7, 134.5, 136.2, 177.4 ppm; IR ($CDCl_3$): 3237, 2094, 1638, 1264, 1072, 1072, 1031, 696 cm^{-1}.

4.3.5. Synthesis of 1-(4-Methoxy-phenyl)-propynone. 1-(4-Methoxy-phenyl)-prop-2-yn-1-ol (2.74 g, 16.8 mmol) was used as described above[42] to produce crude 1-(4-methoxy-phenyl)-propynone (2.01 g, 12.5 mmol) in 74% yield. ^1H NMR, ^{13}C NMR, and IR of this compound agree with those reported previously.[46−48] ^1H NMR (400 MHz, $CDCl_3$): δ 3.34 (s, 1H), 3.90 (s, 3H), 6.97 (d, J = 8.8 Hz, 2H), 8.14 (d, J = 8.8 Hz, 2H) ppm; ^{13}C NMR (100 MHz, $CDCl_3$): δ 55.6, 80.0, 80.4, 114.0, 129.6, 132.2, 164.8, 176.0 ppm; IR ($CDCl_3$): 3251, 2991, 2093, 1640, 1599, 1024, 840, 686 cm^{-1}.

4.3.6. Synthesis of 1-(4-Chloro-phenyl)-propynone. 1-(4-Chloro-phenyl)-propynone (1.7 g, 10.3 mmol) was used as described above[42] to produce crude 1-(4-methoxy-phenyl)-prop-2-yn-1-ol (1.46 g, 8.9 mmol) in 86% yield. The NMR spectra of this compound were similar to those reported.[47−50] ^1H NMR ($CDCl_3$, 400 MHz): δ 3.46 (s, 1H), 7.49 (d, J = 8 Hz, 2H), 8.10 (d, J = 8 Hz, 2H) ppm; ^{13}C NMR (100 MHz, $CDCl_3$): δ 81.2, 81.3, 131.8, 133.4, 133.9, 134.5, 175.9 ppm; IR ($CDCl_3$): 3225, 2088, 1652, 1588, 1564, 1462, 1432, 1235, 1136, 1040, 999, 730, 675, 626 cm^{-1}; GC/MS (EI): m/z 166, 165, 164, 139, 138, 137, 136 (100), 111, 101, 85, 75.

4.3.7. Synthesis of 3,3-Dibromo-1-phenyl-propan-1-one. 3,3-Dibromo-1-phenyl-propan-1-one was synthesized following the procedure reported by Sanseverino et al. with some modifications.[49] 1-Phenyl-propynone (1.38 g, 10.6 mmol) was dissolved in dichloromethane (25 mL) and kept at −8 °C, and SiO_2 (6.36 g, 106 mmol, 10 equiv) was added, followed by dropwise addition of PBr_3 (1.924 g, 7.1 mmol, 0.66 equiv) in dichloromethane (10 mL) using a dropping funnel over a period of 10 min. The mixture was stirred for 20 h, the SiO_2 was filtered off, and the solution dried. The solvent was removed under vacuum to yield crude 3,3-dibromo-1-phenyl-propan-1-one (2.82 g, 9.6 mmol, 91% yield). The product was characterized using ^1H NMR, ^{13}C NMR, IR, and MS spectroscopy. The NMR and IR spectra are consistent with literature values.[50] ^1H NMR (400 MHz, $CDCl_3$): δ 4.19 (d, J = 6.7 Hz, 2H), 6.20 (t, J = 6.7 Hz, 1H), 7.51 (t, J = 7.6 Hz, 2H), 7.63 (t, J = 7.4 Hz, 1H), 7.96 (d, J = 7.6 Hz, 2H) ppm; ^{13}C NMR (100 MHz, $CDCl_3$): δ 36.7, 53.3, 128.2, 128.9, 134.0, 135.7, 194.3 ppm. IR ($CDCl_3$): 1684, 1598, 1580, 1347, 1263, 1219, 755, cm^{-1}; HRMS: m/z calculated for $C_9H_8O_2Br_2Na^+$ $[M + Na]^+$, 314.8819; found, 314.8738; m/z calculated for $C_9H_8O_2Br_2H^+$ $[M + H]^+$, 292.9000; found, 292.9025.

4.3.8. Synthesis of 3,3-Dibromo-1-(4-methoxy-phenyl)-propan-1-one. Synthesis of 3,3-dibromo-1-(phenyl)-propan-1-one was accomplished by a similarly modified Sanseverino procedure as described above.[49] A reaction of 1-(4-methoxy-phenyl)-propynone (2.01 g, 12.5 mmol) resulted in crude 3,3-dibromo-1-(4-methoxy-phenyl)-propan-1-one (3.54 g, 11.0 mmol, 88% yield). The product was characterized using ^1H NMR, ^{13}C NMR, IR, and MS spectroscopy. ^1H NMR (400 MHz, $CDCl_3$): δ 3.89 (s, 3H), 4.13 (d, J = 6.4 Hz, 2H), 6.19 (t, J = 6.4 Hz, 1H), 6.97 (d, J = 8.8 Hz, 2H), 7.94 (d, J = 8.8 Hz, 2H) ppm; ^{13}C NMR ($CDCl_3$, 100 MHz): δ 37.3, 52.9, 55.6, 114.1, 128.8, 130.7, 164.2, 192.8 ppm; IR: 1673, 1599, 1574, 1463, 1421, 1398, 1346, 1318, 1311, 1258, 1223, 785, cm^{-1}; HRMS: m/z calculated for $C_{10}H_{10}O_2Br_2Na^+$ $[M + Na]^+$, 344.89193; found, 344.89206.

4.3.9. Synthesis of 3,3-Dibromo-1-(4-chloro-phenyl)-propan-1-one. We followed the same procedure as that for the synthesis of 3,3-dibromo-1-(phenyl)-propan-1-one.[49] A reaction of 1-(4-methoxy-phenyl)-propynone (2.01 g, 12.5 mmol) resulted in crude 3,3-dibromo-1-(4-chloro-phenyl)-propan-1-one (2.0 g, 6.1 mmol, 69% yield). ^1H NMR (400 MHz, $CDCl_3$): δ 4.19 (d, J = 6.8 Hz, 1H), 6.17 (t, J = 6.8 Hz, 1H), 7.48 (d, J = 7.8 Hz, 2H) 7.99 (d, J = 7.8 Hz, 2H) ppm; ^{13}C NMR (100 MHz, $CDCl_3$,): δ 36.3, 57.3, 129.8, 130.8, 132.8, 137.6, 197.0 ppm; IR ($CDCl_3$): 1693, 1588, 1569, 1468, 1432, 1344, 1270, 1213, 1073, 1040, 979, 757, 626, 584 cm^{-1}; GC/MS (EI): m/z 248, 246, 244, 218, 165, 139 (100), 133, 111, 105, 85, 75. RMS: m/z calculated for $C_9H_7ONaClBr_2$ $[M + Na]^+$, 346.8450; found, 346.8452.

4.3.10. Synthesis of 3-Azido-1-phenyl-propenone (1a). 3,3-Dibromo-1-phenyl-propan-1-one (1.69 g, 5.8 mmol) was dissolved in 20 mL of methanol and 20 mL of acetone at 0 °C. NaN_3 (1.01 g, 15.5 mmol, 5 equiv) dissolved in a minimal amount of water (∼5 mL) was added to the solution. The mixture was stirred for ∼1 h. The solvent was removed under vacuum, and the resulting residue was extracted with diethyl ether (50 mL). The ether layer was washed twice with water (100 mL) and once with saturated brine (100 mL) and dried over anhydrous $MgSO_4$. The solvent was evaporated under vacuum to give crude 3-azido-1-phenyl-propenone (**1a**) (0.710 g, 4.1 mmol, 71% yields). The crude was recrystallized from dichloromethane to give pale yellow crystals. The product was characterized using ^1H NMR, ^{13}C NMR, IR, and MS spectroscopy. Mp (observed): 78−84 °C (lit.;[51] 87−87.5 °C). ^1H NMR (400 MHz, $CDCl_3$): δ 6.77 (d, J = 13.2 Hz, 1H), 7.48 (t, J = 7.6 Hz, 2H), 7.50 (d, J = 13.2 Hz, 1H), 7.58 (t, J = 7.4 Hz, 1H), 7.92 (d, J = 7.2 Hz, 2H) ppm; ^{13}C NMR (100 MHz, $CDCl_3$): δ 113.2, 128.2, 128.7, 133.0, 137.7, 144.9, 188.8 ppm; IR: 3069, 2133, 1657, 1596, 1575, 1448, 1253, 1215, 1018, 950, 773, 682, 644 cm^{-1}. HRMS: m/z calculated for $C_9H_7N_3ONa^+$ $[M + Na]^+$, 196.04813; found, 196.04816.

4.3.11. Synthesis of 3-Azido-1-(4-methoxy-phenyl)-propenone (1b). The synthesis for **1b** was analogous to that for **1a**. 3,3-Dibromo-1-(4-methoxy-phenyl)-propan-1-one (1.43 g, 4.4 mmol) resulted in crude 3-azido-1-(4-methoxy-phenyl)-propenone (**1b**) (0.790 g, 3.9 mmol, 88% yields). The crude was recrystallized from dichloromethane and yielded pale-yellow crystals which were characterized using ^1H NMR, ^{13}C NMR, IR, and MS spectroscopy. Mp (observed): 105−108 °C (lit.;[51] 109−110 °C). ^1H NMR (400 MHz, $CDCl_3$): δ 3.88 (s, 3H), 6.76 (d, J = 13 Hz, 1H), 6.95 (d, J = 8.8 Hz, 2H), 7.48 (d, J = 13 Hz, 1H), 7.92 (d, J = 8.8 Hz, 2H) ppm; ^{13}C NMR (100 MHz, $CDCl_3$): δ 55.5, 113.0, 113.9, 130.6, 144.0, 163.6, 187.1 ppm; IR: 3045, 2138, 1658, 1592, 1574, 1515, 1256, 1226, 1172, 1024, 954, 822, 779, 599 cm^{-1}. HRMS: m/z calculated for $C_{10}H_9N_3O_2Na^+$ $[M + Na]^+$, 226.05870; found, 226.05873.

4.3.12. Synthesis of 3-Azido-1-(4-chloro-phenyl)-propenone (1c). The synthesis of **1c** was similar to that described for **1a**. 3,3-Dibromo-1-(4-chloro-phenyl)-propan-1-one (2.0 g, 6.1 mmol) resulted in crude 3-azido-1-(4-chloro-phenyl)-propenone (**1c**) (0.68 g, 5.4 mmol) in 89% yield. Mp (observed): 93−98 °C (lit.;[51] 98−99 °C). ^1H NMR (400 MHz, $CDCl_3$): δ 6.37 (d, J = 14 Hz, 1H), 7.47 (d, J = 8.8 Hz, 2H) 7. 53 (d, J = 14 Hz, 1H), 7.86 (d, J = 8.8 Hz, 2H) ppm; ^{13}C NMR (100 MHz, $CDCl_3$): δ 117.5, 129.6, 131.2, 136.0, 139.5, 145.4, 187.4 ppm; IR: 3051, 2126, 1660, 1590, 1568, 1254, 1213, 1091, 1013, 823 cm^{-1}; GC/MS (EI): m/z 181, 180, 179, 151, 141, 140, 139, 126, 125, 124, 116, 113, 112, 111, 89, 85, 75, 68, 64.

4.4. Photolytic Studies. *4.4.1. Photolysis of 1a in Chloroform-d.* A solution of **1a** (14 mg, 0.08 mmol) in $CDCl_3$ (1 mL) was purged with argon for 5 min and photolyzed via a Pyrex filter for up to 24 h at 298 K. ^1H NMR and GC analysis of the reaction mixture showed the formation of **3a**, **4a**, and **5a**. The products were characterized by GC-MS chromatography and ^1H NMR, ^{13}C NMR, and IR spectroscopy of the reaction mixture. The spectral data of **4a** and **5a** match with those reported in the literature.[21−25] 2-Phenyl-2*H*-azirine (**3a**): ^1H NMR (400 MHz, $CDCl_3$,): δ 3.47 (d, J = 2 Hz, 1H), 7.44−7.55 (m, 3H), 8.06 (d, J = 8.4 Hz, 2H), 9.57 (d, J = 2 Hz, 1H) ppm; ^{13}C NMR (100 MHz, $CDCl_3$,): δ 28.4, 128.3, 128.8, 133.6, 136.9, 152.4, 197.4 ppm; 5-Phenyl-1,2-oxazole (**4a**): ^1H NMR (400 MHz, $CDCl_3$): δ 6.53 (d, J = 1.6 Hz, 1H), 7.44−7.55 (m, 2H), 7.61−7.69 (m, 1H), 7.79−7.82 (m, 2H), 8.30 (d, J = 1.6 Hz, 1H) ppm; ^{13}C NMR (100 MHz, $CDCl_3$): δ 98.7, 125.9, 127.3, 129.0, 130.2, 150.9, 169.4 ppm; 3-Oxo-3-phenylpropanenitrile (**5a**): ^1H NMR (400 MHz, $CDCl_3$): δ 4.10 (s, 2H), 7.53 (t, J = 7.2 Hz, 2H), 7.67 (t, J = 7.2 Hz, 1H), 7.93 (d, J = 7.2 Hz, 2H) ppm; ^{13}C NMR (100 MHz, $CDCl_3$): δ 29.4, 113.8, 128.5, 129.2, 134.3, 134.8, 187.1 ppm. IR ($CDCl_3$): 2263, 1689 cm^{-1}.

4.4.2. Photolysis of 1b in Chloroform-d. A solution of **1b** (20 mg, 0.1 mmol) in $CDCl_3$ (1 mL) was purged with argon for 5 min and photolyzed via a Pyrex filter for up to 24 h at 298 K. GC and NMR analysis of the reaction mixture showed the formation of **3b**, **4b**, and **5b**. The products were characterized by GC-MS chromatography and ^1H NMR, ^{13}C NMR, and IR spectroscopy of the reaction mixture. The spectral data for **4b** and **5b** match with those reported in the literature.[21−25] 2-(4-Methoxy-phenyl)-2*H*-azirine (**3b**): ^1H NMR

https://dx.doi.org/10.1021/jacs.0c07830
J. Am. Chem. Soc. 2020, 142, 18565−18575

(400 MHz, $CDCl_3$): δ 3.43 (d, J = 2.0 Hz, 1H), 3.86−3.89 (m, 3H), 6.97−7.00 (m, 2H), 8.057 (d, J = 8.8 Hz), 9.57 (d, J = 2.0 Hz, 1H) ppm; ^{13}C NMR (100 MHz, $CDCl_3$,): δ 28.0, 55.5, 114.0, 130.0, 130.6, 152.9, 163.9, 195.6 ppm. IR ($CDCl_3$): 1663 cm^{-1}. 5-(4-Methoxy-phenyl)-1,2-oxazole (**4b**): ^{1}H NMR (400 MHz, $CDCl_3$): δ 3.86 (s, 3H), 6.40 (d, J = 1.6 Hz, 1H), 6.97−7.00 (m, 2H), 7.74 (d, J = 8.8 Hz, 2H), 8.25 (d, J = 2.0 Hz, 1H) ppm; ^{13}C NMR (100 MHz, $CDCl_3$): δ 55.4, 97.3, 114.4, 120.2, 127.5, 150.8, 161.1, 169.3 ppm.; IR ($CDCl_3$): 3014, 2946, 2840, 1599, 1462, 826 cm^{-1}; GC/MS (EI): m/z 175 (M, 100%), 160, 135, 120, 107, 92, 77, 63, 51. 3-Oxo-3-(4-methoxy-phenyl) propanenitrile (**5b**): ^{1}H NMR (400 MHz, $CDCl_3$,): δ 3.90 (s, 3H), 4.03 (s, 2H), 6.98 (d, J = 8.8 Hz, 2H), 7.90 (d, J = 8.8 Hz, 2H) ppm; ^{13}C NMR ($CDCl_3$, 100 MHz): δ 29.0, 55.7, 114.1, 114.3, 127.5, 130.9, 164.7, 185.4 ppm. IR ($CDCl_3$): 2260, 1682 cm^{-1}.

*4.4.3. Photolysis of **1c** in Chloroform-d.* A solution of **1c** in $CDCl_3$ was purged with argon for 5 min and photolyzed via a Pyrex filter for up to 24 h at 298 K. GC analysis of the reaction mixture showed the formation of **3c**, **4c**, and **5c**. The products were characterized by ^{1}H NMR, ^{13}C NMR, and IR spectroscopy of the reaction mixture. The spectral data for **4c** and **5c** match with those reported in the literature.[21−25] 2-(4-Chloro-phenyl)-2*H*-azirine (**3c**): ^{1}H NMR (400 MHz, $CDCl_3$): δ 3.42 (d, J = 2.4 Hz, 1H), 7.44−7.54 (m, 2H), 7.87 (d, J = 8.4 Hz, 2H), 9.56 (d, J = 2.0 Hz, 1H) ppm; ^{13}C NMR (100 MHz, $CDCl_3$): 28.3, 129.8, 131.5, 135.1, 140.1, 152.2, 196.2 ppm. 5-(4-Chloro-phenyl)-1,2-oxazole (**4c**): ^{1}H NMR (400 MHz, $CDCl_3$): δ 6.52 (d, J = 2 Hz, 1H), 7.46 (d, J = 8.4, 2H), 7.74 (d, J = 8.4, 2H), 8.30 (d, J = 1.6 Hz, 1H) ppm; ^{13}C NMR (100 MHz, $CDCl_3$): δ 99.0, 125.7, 127.2, 129.3, 136.3, 150.9, 168.3 ppm. 3-Oxo-3-(4-chloro-phenyl)propanenitrile (**5c**): ^{1}H NMR (400 MHz, $CDCl_3$): δ 4.06 (s, 2H), 7.51 (d, J = 8.4 Hz, 2H), 7.87 (d, J = 8.4 Hz, 2H) ppm; ^{13}C NMR (100 MHz, $CDCl_3$,): δ 29.4, 113.4, 129.7, 129.9, 132.5, 141.5, 186.0 ppm.

*4.4.4. Solid-State Photolysis of Vinyl Azides **1a−1c**.* Crystals of each vinyl azide (5−10 mg) were crushed between two microscope slides and exposed to either a mercury arc lamp in Pyrex or 400 nm LED for 1 h, and the sample was analyzed by ^{1}H NMR and IR spectroscopy. In each case, the photoproduct formed was the corresponding azirine **3**.

4.5. Thermolysis of Vinyl Azides 1a−1c. NMR tubes were charged with solutions of **1a−1c** (4.0 mg) in $CDCl_3$ (0.5 mL). The NMR tubes were heated in a preheated oil bath at 70 °C for 10 min. ^{1}H NMR, ^{13}C NMR, and IR spectroscopy of the reaction mixture showed the formation of the corresponding azirines **3** and cyanides **5**.

4.6. Nanoindentation. The nanoindentation measurements on **1b** and **1c** were performed with an Agilent G200 nanoindenter equipped with an XP head, using a Berkovitch diamond indenter. Each indentation was performed using the continuous stiffness method to a depth of 1000 nm with a strain rate of 0.05, an amplitude of 2 nm, and a frequency of 45 Hz.[52] Prior to the indentation, the stiffness and the geometry of the tip were determined by using a Corning 7980 silica reference sample (Nanomechanics S1495-25). In order to ensure that the tip was fully engaged, the modulus was measured between 200 and 1000 nm. The value of the Poisson's ratio was assumed to be 0.30. A comparison of the young's modulus of **1b** and **1c** crystals with a very few relevant recent photoresponsive systems was provided in Supporting Information Table S10.[53−55]

4.7. Crystal Movement Video Specifications. Crystals of vinyl azides **1a**, **1b**, and **1c** were grown from a dichloromethane solution at 0 °C and placed on the stage of a Keyence VHX-1000E digital microscope. The photolysis was initiated using a LuzChem LED array with blue light, as well as two LEDs of 365 and 400 nm outputs. The photolysis was recorded over the course of a few minutes of exposure for Supporting Information videos 2−8 and 60 min for video 1.

■ ASSOCIATED CONTENT

Supporting Information

The Supporting Information is available free of charge at https://pubs.acs.org/doi/10.1021/jacs.0c07830.

Spectra for characterization of **1a−c** and the photoproducts; DFT calculation data (PDF)

Vinyl azide **1a** exposed to a 400nm LED and monitored using an optical microscope equipped with a camera (AVI)

Evolution of N_2 by coverage of **1a** crystals with mineral oil followed by irradiation (AVI)

Crystals of **1b** bending, expanding, and cracking (AVI)

Jumping of **1b** crystals if not restrained (AVI)

Formation of a gas bubble could be observed in the **1b** crystal prior to cracking (AVI)

Crystals of **1c** bending, expanding, and cracking upon exposure to light (AVI)

Jumping of **1c** crystals (AVI)

Crystals of **1c** in oil showing no N_2 release until cracks generated (AVI)

Crystallographic data for **1a−1c** (CIF)

■ AUTHOR INFORMATION

Corresponding Authors

Anna D. Gudmundsdottir − *Department of Chemistry, University of Cincinnati, Cincinnati, Ohio 45221-0172, United States;* orcid.org/0000-0002-5420-4098; Email: anna.gudmundsdottir@uc.edu

Pančе Naumov − *New York University Abu Dhabi, Abu Dhabi, United Arab Emirates;* orcid.org/0000-0003-2416-6569; Email: pance.naumov@nyu.edu

Authors

Dylan J. Shields − *Department of Chemistry, University of Cincinnati, Cincinnati, Ohio 45221-0172, United States*

Durga Prasad Karothu − *New York University Abu Dhabi, Abu Dhabi, United Arab Emirates;* orcid.org/0000-0001-5956-6496

Karthik Sambath − *Department of Chemistry, University of Cincinnati, Cincinnati, Ohio 45221-0172, United States;* orcid.org/0000-0002-9876-7167

Ranaweera A. A. Upul Ranaweera − *Department of Chemistry, University of Cincinnati, Cincinnati, Ohio 45221-0172, United States;* orcid.org/0000-0003-1614-1919

Stefan Schramm − *New York University Abu Dhabi, Abu Dhabi, United Arab Emirates*

Alexander Duncan − *Department of Chemistry, University of Cincinnati, Cincinnati, Ohio 45221-0172, United States*

Benjamin Duncan − *Department of Chemistry, University of Cincinnati, Cincinnati, Ohio 45221-0172, United States*

Jeanette A. Krause − *Department of Chemistry, University of Cincinnati, Cincinnati, Ohio 45221-0172, United States*

Complete contact information is available at: https://pubs.acs.org/10.1021/jacs.0c07830

Author Contributions

‖K.S. and R.A.A.U.R. contributed equally.

Notes

The authors declare no competing financial interest.

CCDC 2015372−2015374 contain the crystallographic data in CIF format. These data can be obtained, free of charge via http://www.ccdc.cam.ac.uk/products/csd/request/ (or from the Cambridge Crystallographic Data Centre, 12 Union Road, Cambridge CB2 1EZ, U.K.; Fax: 44−1223−336033 or e-mail: deposit@ccdc.cam.ac.uk).

■ ACKNOWLEDGMENTS

We thank the NSF (CHE-1800140 and MRI:CHE-1726092) and OSC (PES0597) for their support. D.J.S. acknowledges Doctoral Enhancement, Stecke, and Twitchell Fellowships; R.A.A.U.R. acknowledges Harry B. Mark, Ann P. Villalobos, and URC Fellowships. Funding for the SMART6000 CCD diffractometer was through NSF-MRI grant CHE-0215950. Synchrotron X-ray data were collected through the SCrALS (Service Crystallography at Advanced Light Source) program at Beamline 11.3.1 at the Advanced Light Source (ALS), Lawrence Berkeley National Laboratory. The ALS is supported by the U.S. Department of Energy, Office of Energy Sciences Materials Sciences Division, under Contract DE-AC02-05CH11231. This research was partially carried out using the Core Technology Platform resources at the New York University Abu Dhabi.

■ REFERENCES

(1) Yu, Y.; Nakano, M.; Ikeda, T. Directed bending of a polymer film by light. *Nature* **2003**, *425*, 145−145.
(2) Al-Kaysi, R. O.; Tong, F.; Al-Haidar, M.; Zhu, L.; Bardeen, C. J. Highly branched photomechanical crystals. *Chem. Commun.* **2017**, *53*, 2622−2625.
(3) Ikeda, T.; Mamiya, J.-i.; Yu, Y. Photomechanics of liquid-crystalline elastomers and other polymers. *Angew. Chem., Int. Ed.* **2007**, *46*, 506−528.
(4) Juodkazis, S.; Mukai, N.; Wakaki, R.; Yamaguchi, A.; Matsuo, S.; Misawa, H. Reversible phase transitions in polymer gels induced by radiation forces. *Nature* **2000**, *408*, 178−181.
(5) Commins, P.; Desta, I. T.; Karothu, D. P.; Panda, M. K.; Naumov, P. Crystals on the move: Mechanical effects in dynamic solids. *Chem. Commun.* **2016**, *52*, 13941−13954.
(6) Ahmed, E.; Karothu, D. P.; Naumov, P. Crystal adaptronics: Mechanically reconfigurable elastic and superelastic molecular crystals. *Angew. Chem., Int. Ed.* **2018**, *57*, 8837−8846.
(7) Karothu, D. P.; Halabi, J. M.; Li, L.; Colin-Molina, A.; Rodríguez-Molina, B.; Naumov, P. Global performance indices for dynamic crystals as organic thermal actuators. *Adv. Mater.* **2020**, *32*, 1906216.
(8) Ahmed, E.; Karothu, D. P.; Warren, M.; Naumov, P. Shape memory effects in molecular crystals. *Nat. Commun.* **2019**, *10*, 3723.
(9) Naumov, P.; Karothu, D. P.; Ahmed, E.; Catalano, L.; Commins, P.; Halabi, J. M.; Al-Handawi, M. B.; Li, L. The Rise of the Dynamic Crystals. *J. Am. Chem. Soc.* **2020**, *142*, 13256−13272.
(10) Naumov, P.; Chizhik, S.; Panda, M. K.; Nath, N. K.; Boldyreva, E. Mechanically responsive molecular crystals. *Chem. Rev.* **2015**, *115*, 12440−12490.
(11) Naumov, P.; Sahoo, S. C.; Zakharov, B. A.; Boldyreva, E. V. Dynamic single crystals: Kinematic analysis of photoinduced crystal jumping (the photosalient effect). *Angew. Chem., Int. Ed.* **2013**, *52*, 9990−9995.
(12) Ovcharenko, V. I.; Sagdeev, R. Z. Molecular ferromagnets. *Russ. Chem. Rev.* **1999**, *68*, 345−363.
(13) Ovcharenko, V. I.; Fokin, S. V.; Romanenko, G. V.; Korobkov, I. V.; Rey, P. Synthesis of vicinal bishydroxylamin. *Russ. Chem. Bull.* **1999**, *48*, 1519−1525.
(14) Ovcharenko, V. I.; Fokin, S. V.; Fursova, E. Y.; Kuznetsova, O. V.; Tretyakov, E. V.; Romanenko, G. V.; Bogomyakov, A. S. Jumping crystals": Oxygen-evolving metal-nitroxide complexes. *Inorg. Chem.* **2011**, *50*, 4307−4312.
(15) Chevilott, P. F.; Edwards, W. F. *Ann. Chim. Phys.* **1817**, *4*, 287.
(16) Chevilott, P. F.; Edwards, W. F. *Ann. Chim. Phys.* **1818**, *8*, 333.
(17) Boldyrev, V. V. Mechanochemical Processes with the Reaction-Induced Mechanical Activation. Chemo-Mechanochemical Effect. *Russ. Chem. Bull.* **2018**, *67*, 933−948.
(18) Oates, W. A.; Todd, D. D. *Proceedings of the First Australian Conference on Electron Microscopy*; Hobart: 1965; p 88.
(19) Bowden, F. P.; Yoffe, A. D. Fast Reactions in Solids. *Angew. Chem.* **1959**, *71*, 752.
(20) Sato, S. Azirines. IV. The photolysis of β-azidovinyl ketones. *Bull. Chem. Soc. Jpn.* **1968**, *41*, 2524−2525.
(21) Rosa, F. A.; Machado, B.; Bonacorso, H. G.; Zanatta, N.; Martins, M. A. P. Reaction of β-dimethylaminovinyl ketones with hydroxylamine: A simple and useful method for synthesis of 3- and 5-substituted isoxazoles. *J. Heterocycl. Chem.* **2008**, *45*, 879−885.
(22) Isomura, K.; Hirose, Y.; Shuyama, H.; Abe, S.; Ayabe, G.-i; Taniguchi, H. Unusual formation of oxazoles by base- or acid-catalyzed ring opening of 2-acyl-2*H*-azirines. *Heterocycles* **1978**, *9*, 1207−1216.
(23) James, M. L.; Fulton, R. R.; Henderson, D. J.; Eberl, S.; Meikle, S. R.; Thomson, S.; Allan, R. D.; Dolle, F.; Fulham, M. J.; Kassiou, M. Synthesis and *in vivo* evaluation of a novel peripheral benzodiazepine receptor PET radioligand. *Bioorg. Med. Chem.* **2005**, *13*, 6188−6194.
(24) Gøgsig, T. M.; Nielsen, D. U.; Lindhardt, A. T.; Skrydstrup, T. Palladium catalyzed carbonylative Heck reaction affording monoprotected 1,3-ketoaldehydes. *Org. Lett.* **2012**, *14*, 2536−2539.
(25) Shen, J.; Yang, D.; Liu, Y.; Qin, S.; Zhang, J.; Sun, J.; Liu, C.; Liu, C.; Zhao, X.; Chu, C.; Liu, R. Copper-catalyzed aerobic oxidative coupling of aromatic alcohols and acetonitrile to β-ketonitriles. *Org. Lett.* **2014**, *16*, 350−353.
(26) Nesmeyanov, A. N.; Rybinskaya, M. I.; Kelekhsaeva, T. G. Effect of stereochemical and electronic factors on the decomposition and rearrangement of β-azidovinyl ketones. *Bull. Acad. Sci. USSR, Div. Chem. Sci.* **1969**, *18*, 787−790.
(27) Hirshfeld, F. L.; Schmidt, G. M. J. Topochemical control of solid-state polymerization. *J. Polym. Sci., Part A: Gen. Pap.* **1964**, *2*, 2181−2190.
(28) Sarkar, S. K.; Sawai, A.; Kanahara, K.; Wentrup, C.; Abe, M.; Gudmundsdottir, A. D. Direct detection of a triplet vinylnitrene, 1,4-naphthoquinone-2-ylnitrene, in solution and cryogenic matrices. *J. Am. Chem. Soc.* **2015**, *137*, 4207−4214.
(29) Rajam, S.; Murthy, R. S.; Jadhav, A. V.; Li, Q.; Keller, C.; Carra, C.; Pace, T. C. S.; Bohne, C.; Ault, B. S.; Gudmundsdottir, A. D. Photolysis of (3-methyl-2*H*-azirin-2-yl)-phenylmethanone: Direct detection of a triplet vinylnitrene intermediate. *J. Org. Chem.* **2011**, *76*, 9934−9945.
(30) Simoncelli, S.; Kuzmanich, G.; Gard, M. N.; Garcia-Garibay, M. A. Photochemical reaction mechanisms and kinetics with molecular nanocrystals: Surface quenching of triplet benzophenone nanocrystals. *J. Phys. Org. Chem.* **2010**, *23*, 376−381.
(31) Becke, A. D. Density-functional thermochemistry. III. The role of exact exchange. *J. Chem. Phys.* **1993**, *98*, 5648−5652.
(32) Lee, C.; Yang, W.; Parr, R. G. Development of the Colle-Salvetti correlation-energy formula into a functional of the electron density. *Phys. Rev. B: Condens. Matter Mater. Phys.* **1988**, *37*, 785−789.
(33) Mackenzie, C. F.; Spackman, P. R.; Jayatilaka, D.; Spackman, M. A. *CrystalExplorer* model energies and energy frameworks: Extension to metal coordination compounds, organic salts, solvates and open-shell systems. *IUCrJ* **2017**, *4*, 575−587.
(34) Frisch, M. J.; Trucks, G. W.; Schlegel, H. B.; Scuseria, G. E.; Robb, M. A.; Cheeseman, J. R.; Scalmani, G.; Barone, V.; Petersson, G. A.; Nakatsuji, H.; Li, X.; Caricato, M.; Marenich, A. V.; Bloino, J.; Janesko, B. G.; Gomperts, R.; Mennucci, B.; Hratchian, H. P.; Ortiz, J. V.; Izmaylov, A. F.; Sonnenberg, J. L.; Williams-Young, D.; Ding, F.; Lipparini, F.; Egidi, F.; Goings, J.; Peng, B.; Petrone, A.; Henderson, T.; Ranasinghe, D.; Zakrzewski, V. G.; Gao, J.; Rega, N.; Zheng, G.; Liang, W.; Hada, M.; Ehara, M.; Toyota, K.; Fukuda, R.; Hasegawa, J.; Ishida, M.; Nakajima, T.; Honda, Y.; Kitao, O.; Nakai, H.; Vreven, T.; Throssell, K.; Montgomery, J. A., Jr.; Peralta, J. E.; Ogliaro, F.; Bearpark, M. J.; Heyd, J. J.; Brothers, E. N.; Kudin, K. N.; Staroverov, V. N.; Keith, T. A.; Kobayashi, R.; Normand, J.; Raghavachari, K.; Rendell, A. P.; Burant, J. C.; Iyengar, S. S.; Tomasi, J.; Cossi, M.; Millam, J. M.; Klene, M.; Adamo, C.; Cammi, R.; Ochterski, J. W.; Martin, R. L.; Morokuma, K.; Farkas, O.; Foresman, J. B.; Fox, D. J. *Gaussian 16*, Revision C.01; Gaussian, Inc.: Wallingford, CT, 2016.

https://dx.doi.org/10.1021/jacs.0c07830
J. Am. Chem. Soc. 2020, 142, 18565−18575

(35) Foresman, J. B.; Head-Gordon, M.; Pople, J. A.; Frisch, M. J. Toward a systematic molecular orbital theory for excited states. *J. Phys. Chem.* **1992**, *96*, 135−149.
(36) Bauernschmitt, R.; Ahlrichs, R. Treatment of electronic excitations within the adiabatic approximation of time dependent density functional theory. *Chem. Phys. Lett.* **1996**, *256*, 454−464.
(37) Mennucci, B.; Tomasi, J.; Cammi, R.; Cheeseman, J. R.; Frisch, M. J.; Devlin, F. J.; Gabriel, S.; Stephens, P. J. Polarizable continuum model (PCM) calculations of solvent effects on optical rotations of chiral molecules. *J. Phys. Chem. A* **2002**, *106*, 6102−6113.
(38) Gonzalez, C.; Schlegel, H. B. Reaction path following in mass-weighted internal coordinates. *J. Phys. Chem.* **1990**, *94*, 5523−5527.
(39) Gonzalez, C.; Schlegel, H. B. J. An improved algorithm for reaction path following. *J. Chem. Phys.* **1989**, *90*, 2154−2161.
(40) Muthukrishnan, S.; Sankaranarayanan, J.; Klima, R. F.; Pace, T. C. S.; Bohne, C.; Gudmundsdottir, A. D. Intramolecular H-atom abstraction in γ-azido-butyrophenones: Formation of 1,5 ketyl iminyl radicals. *Org. Lett.* **2009**, *11*, 2345−2348.
(41) Chassaing, S.; Kueny-Stotz, M.; Isorez, G.; Brouillard, R. Rapid preparation of 3-deoxyanthocyanidins and novel dicationic derivatives: New insight into an old procedure. *Eur. J. Org. Chem.* **2007**, *2007*, 2438−2448.
(42) Pigge, F. C.; Ghasedi, F.; Zheng, Z.; Rath, N. P.; Nichols, G.; Chickos, J. S. Structural characterization of crystalline inclusion complexes formed from 1,3,5-triaroylbenzene derivatives-a new family of inclusion hosts. *J. Chem. Soc., Perkin Trans. 2* **2000**, 2458−2464.
(43) Park, S.; Joo, J. M.; Cho, E. J. Synthesis of β-trifluoromethylated ketones from propargylic alcohols by visible light photoredox catalysis. *Eur. J. Org. Chem.* **2015**, *2015*, 4093−4097.
(44) Kalhor-Monfared, S.; Beauvineau, C.; Scherman, D.; Girard, C. Synthesis and cytotoxicity evaluation of aryl triazolic derivatives and their hydroxymethine homologues against B16 melanoma cell line. *Eur. J. Med. Chem.* **2016**, *122*, 436−441.
(45) Maeda, Y.; Kakiuchi, N.; Matsumura, S.; Nishimura, T.; Kawamura, T.; Uemura, S. Oxovanadium complex-catalyzed aerobic oxidation of propargylic alcohols. *J. Org. Chem.* **2002**, *67*, 6718−6724.
(46) Zheng, M.; Wu, F.; Chen, K.; Zhu, S. Styrene as 4π-component in Zn(II)-catalyzed intermolecular Diels−Alder/Ene tandem reaction. *Org. Lett.* **2016**, *18*, 3554−3557.
(47) Weerasiri, K. C.; Gorden, A. E. V. Oxidation of propargylic alcohols with a 2-quinoxalinol salen copper(II) complex and tert-butyl hydroperoxide. *Eur. J. Org. Chem.* **2013**, *2013*, 1546−1550.
(48) Shi, F.; Luo, S.-W.; Tao, Z.-L.; He, L.; Yu, J.; Tu, S.-J.; Gong, L.-Z. The catalytic asymmetric 1,3-dipolar cycloaddition of ynones with azomethine ylides. *Org. Lett.* **2011**, *13*, 4680−4683.
(49) Sanseverino, A. M.; de Mattos, M. C. S. Hydrobromination of alkenes with PBr_3/SiO_2: A simple and efficient regiospecific preparation of alkyl bromides. *J. Braz. Chem. Soc.* **2001**, *12*, 685−687.
(50) Pirtsch, M.; Paria, S.; Matsuno, T.; Isobe, H.; Reiser, O. $[Cu(dap)_2Cl]$ as an efficient visible-light-driven photoredox catalyst in carbon−carbon bond-forming reactions. *Chem. - Eur. J.* **2012**, *18*, 7336−7340.
(51) Fischer, G. W. Vinyloge acylverbindungen, VII. Synthese und reaktives verhalten vinyloger *N*-Acyl-pyridiniumsalze. *Chem. Ber.* **1970**, *103*, 3470−3488.
(52) Oliver, W. C.; Pharr, G. M. An improved technique for determining hardness and elastic modulus using load and displacement sensing indentation experiments. *J. Mater. Res.* **1992**, *7*, 1564−1583.
(53) Annadhasan, M.; Karothu, D. P.; Chinnasamy, R.; Catalano, L.; Ahmed, E.; Ghosh, S.; Naumov, P.; Chandrasekar, R. Micromanipulation of mechanically compliant organic single-crystal optical microwaveguides. *Angew. Chem., Int. Ed.* **2020**, *59*, 13821−13830.
(54) Mishra, M. K.; Mukherjee, A.; Ramamurty, U.; Desiraju, G. R. Crystal chemistry and photomechanical behavior of 3,4-dimethoxycinnamic acid: correlation between maximum yield in the solid-state topochemical reaction and cooperative molecular motion. *IUCrJ* **2015**, *2*, 653−660.
(55) Sahoo, S. C.; Nath, N. K.; Zhang, L.; Semreen, M. H.; Al-Tel, T. H.; Naumov, P. Actuation based on thermo/photosalient effect: a biogenic smart hybrid driven by light and heat. *RSC Adv.* **2014**, *4*, 7640−7647.

https://dx.doi.org/10.1021/jacs.0c07830
J. Am. Chem. Soc. 2020, 142, 18565−18575